ECRONICON OPEN ACCESS

EC DENTAL SCIENCE
Research Article

Submicron X-Ray Computed Tomography of Human Dentin Treated with Topical Fluoride Modalities

Makoto Asaizumi[1]*, Tomoaki Kato[2], Tetsuya Kuga[2], Nahoko Oode[3], Takehide Oda[3], Tsuguo Sakurada[3], Kris Thomson[4], Tomohiro Tabara[5], and Robert L. Karlinsey[6]

[1]Dr. Makoto Asaizumi Orthodontic Practice, Ban Bldg. 3F. 1-8 Chiyodacho, Mobara, Chiba 297-0023, Japan

[2]Dr. Tetsuya Kuga Dental Practice, 924 Kamiichiba, Mutsuzawamachi, Chouseigun, Chiba 299-4403, Japan

[3]JFE Techno-Research Corporation, 1-1 Minami Wataridacho, Kawasakiku, Kawasaki, Kanagawa 210-0855, Japan

[4]Anatomage, Inc. 303 Almaden Blvd, #700 San Jose, California, 95110, USA

[5]Carl Zeiss Microscopy Japan Co., Ltd., 7 Honshiocho, Shinjukuku, Tokyo 160-0003, Japan

[6]Indiana Nanotech, 7750 Centerstone Drive, Indianapolis, IN 46259, USA

***Corresponding Author**: Dr. Makoto Asaizumi, Ban Bldg. 3F. 1-8 Chiyodacho, Mobara, Chiba 297-0023, Japan.

Received: August 03, 2016; **Published:** September 20, 2016

Abstract

Objective: Characterization studies on demineralized dentin are important in understanding, preventing and addressing dentinal hypersensitivity. Multiple microscopy techniques, including an advanced synchrotron radiation (SR) X-ray computed tomography (CT) experiment, were used to assess the submicron morphology, composition and structure of sound and demineralization human dentin, as well as demineralized dentin treated with three different fluoride formulations.

Methods: Dentin samples were obtained and prepared from extracted human bicuspids and arranged into five groups (N = 5): sound dentin; demineralized dentin; and, demineralized dentin treated with either a 0.2% NaF prophy paste, 1.1% NaF dentifrice or 5% NaF varnish. Specimens were then submitted to an advanced SR X-ray CT technique involving microscope optics providing submicron spatial resolution. Multiple comparison statistical analyses (Tukey HSD, $p < 0.05$) were performed on X-ray linear attenuation coefficients (LACs) for each group. Specimens were further assessed for morphology and composition using digital light microscopy (DLM), field-emission scanning electron microscopy (FE-SEM) and focused ion beam (FIB) techniques. CT, FE-SEM and FIB data files were then imported into software packages to create volume renderings for visualization purposes.

Results: LAC values were obtained via SR X-ray CT and used to estimate mineral concentrations within dentin tubules as well as in the inter-tubular regions. Our investigation yielded region-specific trends in mineral concentrations for sound and demineralized dentin, and demineralized dentin treated with each of the fluoride formulations. Statistical differences were observed among treatment groups as a function of depth into dentin. Complimenting SR X-ray CT, DLM, FE-SEM and FIB provided morphological and compositional detail.

Conclusion: SR X-ray CT provided submicron resolution of tubular and inter-tubular demineralized dentin treated with different fluoride modalities, including a prophy paste, dentifrice and varnish. The use of SR X-ray CT to probe region-specific processes provides important insight into dentinal structure and may find further applications in addressing and understanding dentinal hypersensitivity.

Keywords: *Synchrotron Radiation; X-ray Computed Tomography; Demineralization; Remineralization; Fluoride; Hydroxyapatite; Dentin Tubule; Occlusion*

Introduction

Dentinal hypersensitivity is common worldwide, manifesting especially in periodontal populations where root sensitivity is reported by nearly all categorical patients [1,2]. The etiology of dentinal hypersensitivity is largely but not perfectly understood. The thinning and loss of enamel, especially around the cervical margin, is certainly a dominant factor, while another is the gradual recession of gingiva [1-3]. With the loss of enamel from the crown surfaces, the underlying dentin, which is largely comprised of apatite-like mineral, Type I collagen and water, becomes susceptible to demineralization [4,5]. Similarly, near the pulpal base, the cementum can become compromised as the gingiva recedes, leading to a breakdown in connective tissue [1-5]. As destructive processes including caries, abrasion and erosion progress, the integrity of the dentin mantle weakens, leading to, for instance, patency of tubules. The tubules are a complex structure, comprising fluid, minerals and biological material, and manifest larger diameters near the pulp relative to the dentin-enamel junction [1-5]. When sufficiently demineralized, leakage and/or disruptions of tubular fluid occurs, which in turn affects pulpal nerve receptors [1-4].

Permeability studies have helped identify patency of tubules as a major characteristic of dentinal hypersensitivity [2,6]. The dominant theory supporting permeability studies is known as the hydrodynamic theory, and has supported pursuits of occlusion and demineralization of dentin tubules [1-4,6,7]. Approaches utilizing reliefs (or, replicas) are useful for near-surface assessments but may not provide sufficient subsurface detail [8-10].

One way to characterize the subsurface is the use of X-ray computed tomography (CT), which allows for non-destructive collection of 3D morphologies and internal structures [11-21]. CT images generated during the experiment are expressed as a spatial distribution of the so-called CT values, which have a relation to the X-ray linear attenuation coefficient (LAC) of a material. Three-dimensional internal structures can subsequently be obtained by stacking CT images. While relatively accessible compared to synchrotron sources, conventional CT experiments utilizing polychromatic X-rays require corrections to address method-derived artefacts, and therefore may influence data accuracy [13-16,20]. One way to help improve image quality, and therefore the 'true' characteristics of the material, could be through the use of a synchrotron radiation (SR) source combined with well-characterized X-ray LAC theory-experiment relationships [20]. An SR source provides tunable, monochromatized, and naturally collimated (parallel) X-ray beams that have many advantages for CT, including high-flux density, high signal-to-noise ratios, high spatial resolutions, and monochromatized beams eliminate beam hardening effects (which lead to CT image artifacts), while permitting spatial resolution that allow quantification of LAC values from CT images [11,12,18-20].

Innovations in SR X-ray CT continue to improve the quality CT data, and therefore, LAC values [18-20]. One of the more significant innovations is the inclusion of a Fresnel zone plate (FZP) in the microscope optics to magnify X-ray beams impinging on the detector [17,22,23]. This increased sensitivity enables submicron resolution, and is especially useful in probing composition and structure of small particles, such as the regolith particle samples from the asteroid Itokawa [20]. With respect to tooth structure, the use of FZP in SR X-ray CT experiments has been applied to probe submicron details of water-immersed dentin [17]. However, subsurface investigations of sound and demineralized dentin utilizing SR X-ray CT with an advanced optic arrangement comprising FZP has yet to be performed.

In our previous work, we have probed the microstructure of incipient bovine enamel lesions cycled in an in vitro remineralization model using a conventional and synchrotron radiation (SR) X-ray CT [21,24]. The outcome of those studies demonstrated that only SR X-ray CT was sensitive enough to detect significant microstructural differences in incipient enamel lesions subjected to three different dentifrices, including a fluoride-free dentifrice (Tom's of Maine) along with 0.21% NaF and 1.1% NaF dentifrices (3M Clinpro Tooth Crème and Clinpro 5000, respectively) [21]. The purpose of the present work was to assess dentin structure using SR X-ray CT with the aim of distinguishing differences between sound and initially demineralized dentin, as well as demineralized dentin treated with three different fluoride preparations. The three fluoride preparations used in our study are include a newly developed 0.2% NaF prophy paste containing silica microspheres (DualPro™, Elevate Oral Care, USA), a 1.1% NaF dentifrice containing functionalized TCP (Clinpro™ 5000, 3M Oral

Care, USA), and a 5% NaF varnish (Vanish™ Varnish with TCP, 3M Oral Care, USA) also containing functionalized TCP. The dentifrice and varnish are popular fluoride modalities, contain an optimized combination of fluoride plus functionalized TCP, and have demonstrated efficacy in a variety of laboratory and clinical models [21,24-34]. Using advanced WAXD and SAXS methodologies, we recently demonstrated the fluoride plus functionalized TCP combination leads to nanoscale apatite-like mineral formation that mineralizes and strengthens the subsurface region [35]. Therefore, those observations may bear on any potential benefit observed in the mineralization of weakened dentin. The prophy paste was chosen based on its unique formulation with silica microspheres, which may provide dentinal hypersensitivity benefits via tubule occlusion.

Our SR X-ray CT experiments on dentin samples were performed on the BL47XU beamline of the SPring-8 third-generation synchrotron radiation facility in Hyogo, Japan. Complimenting these evaluations, digital light microscopy, high-resolution field-emission scanning electron microscopy (FE-SEM), and Focused Ion Beam (FIB) techniques were also employed for morphological and elemental assessments. Imaging software was used to construct volume renderings based on CT, FE-SEM and FIB data files.

Materials and Methods

Specimen Preparation, Treatment Groups and Protocol

Human permanent bicuspids were extracted for orthodontic reasons and collected from four independent dental practices (Dr. Kuga; Dr. Nomura; Dr. Yamakura; and, Dr. Asaizumi) in and around Chiba, Japan. Dexterous dentin excisions and sculpting were subsequently performed using a KaVo straight hand piece with a diamond point F4R (Shofu Co. Japan), resulting in tapered human hair-width diameters of about 60 µm and overall lengths about 8 mm. The specimen base was supported with acrylic resin for handling purposes. An example of a dentin specimen is shown in Figure 1, where a 100 µm field of view (FOV) scale box is also shown.

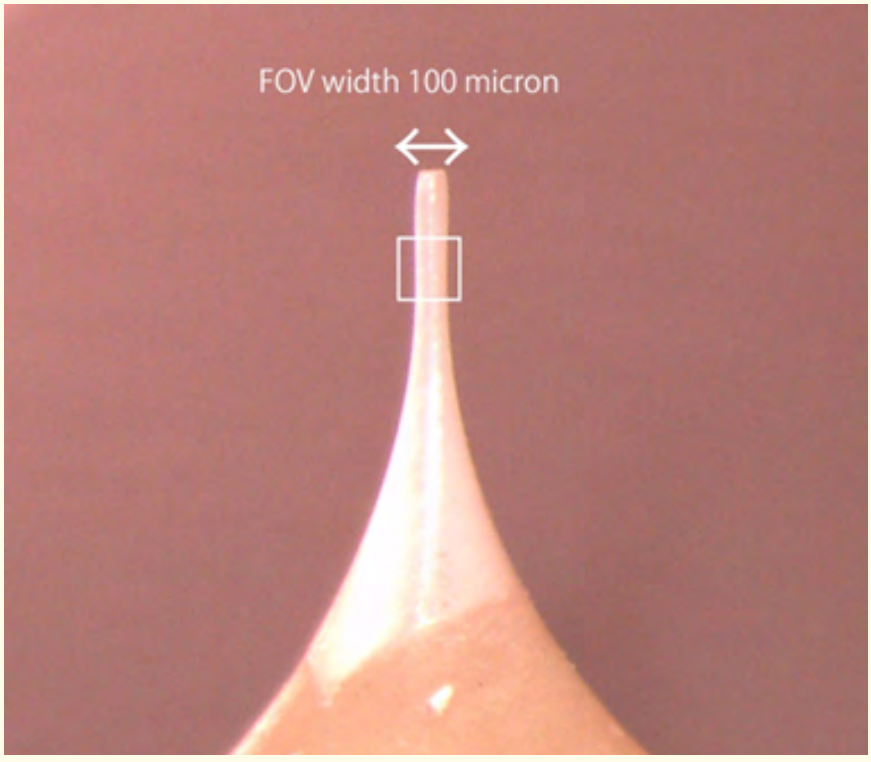

Figure 1: *Representative human dentin specimen sculpted from extracted human bicuspids. Field of view (FOV) scale box corresponds to 100 µm.*

Specimens were then distributed among five groups (N = 5 per group) labeled as follows:

S: Sound dentin for control purposes
D: Demineralized dentin for control purposes

A: Demineralized dentin treated with 0.2% NaF prophy paste (DualPro™, Elevate Oral Care, USA)
B: Demineralized dentin treated with 1.1% NaF dentifrice (Clinpro™ 5000, 3M Oral Care, USA)
C: Demineralized dentin treated with 5% NaF varnish (Vanish™ Varnish with TCP, 3M Oral Care, USA)

The demineralized dentin specimens in groups D, A, B and C were initially exposed to a 1% citric acid (pH = 3.2) challenge for 20 seconds, and then rinsed with distilled water. Each treatment group A, B and C was then subjected to a 3-day protocol outlined in Table 1.

The first two days' events included an acid challenge, treatment and then immersion in stimulated saliva. Due to the delicacy of the dentin specimens, only two 20-second treatments were administered. The treatments were given as follows. Prior to all treatments, the dentin specimens were refreshed with light moistening and gentle puffs of air. Approximately one gram of each group A and B received a couple droplets of distilled water and mixed with plastic spatula on a silica glass slide for 10 seconds for improved workability; for group A, the prophy paste was then gently applied using the Kavo contra-angle hand piece fitted with a rubber cup; for group B, dentin specimens were gently hand-dipped with a rolling action onto the lightly diluted dentifrice sample. A carefully and thinly applied veneer was applied to the dentin specimens in group C. The 1% citric acid solution used to initially demineralize the groups D, A, B and C was also used for all acid challenges, with new solution used for each acid challenge. Paraffin wax chewing for 20 minutes was used to stimulate saliva (pH ~ 7) and was collected from a single source (Dr. M. Asaizumi). On the third day, specimens were only exposed to an acid challenge. In between all events, the specimens were lightly rinsed with distilled water with one exception: preliminary work demonstrated dentin specimens became too delicate for follow-on rinsing once the sticky varnish was applied; in this case, the lightly veneered specimens were then immersed directly into the citric acid solution.

Event	Duration
Acid Challenge #1	20 seconds
Treatment #1	20 seconds
Stimulated Saliva #1	overnight
Acid Challenge #2	2 minutes
Treatment #2	20 seconds
Stimulated Saliva #2	overnight
Acid Challenge #3	20 seconds

Table 1: *Treatment-challenge protocol applied to dentin specimens in groups A, B and C.*

Digital Light Microscopy

All dentin samples were assessed for size and form with digital light microscope model VHX-500 fitted with the VH-Z500 zoom lens (Keyence Corporation, Japan). Bright field reflected light microscopy at 300x magnification for were imaged for each of the five groups prior to synchrotron radiation X-ray and scanning electron microscopy experiments.

SR X-ray CT Measurements

Synchrotron radiation (SR) X-ray computed tomography (CT) experiments were performed at BL47XU of SPring-8 synchrotron radiation facility (Hyogo, Japan). A schematic of the experimental setup is shown in Figure 2, and full details of the experimental arrangement can be found elsewhere [19,20,23]. Within this arrangement, each mounted dentin specimen is positioned as shown in Figure 3.

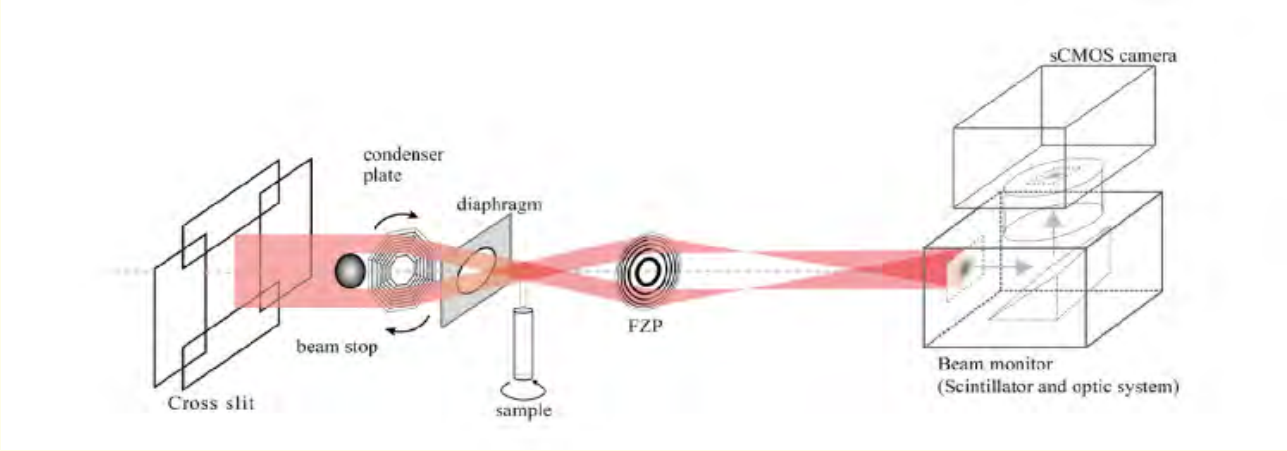

Figure 2: *Schematic of the SR X-ray CT set-up at BL47XU in the SPring-8 synchrotron radiation facility.*

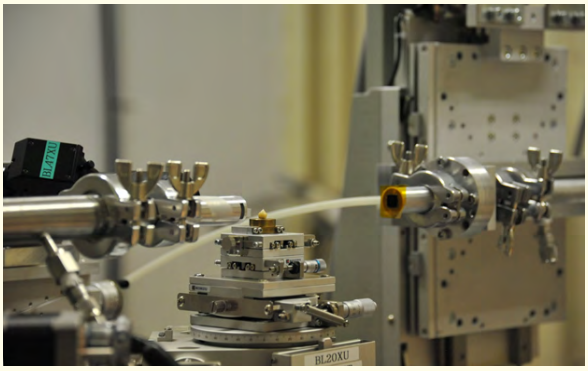

Figure 3: *Example view of dentin sample positioning within the X-ray optical setup at BL47XU. The tapered dentin sample is oriented orthogonal to the X-ray beam axis.*

Notably, this X-ray optic arrangement utilized a Fresnel zone plate (FZP), which magnifies X-ray beams, allowing for submicron resolution [20,22]. The X-ray energy used in these studies was 8 keV, and in this arrangement the resultant CT images had voxel edge lengths of 51 nm. There were 1,500 projection images collected, with the sample rotated over 180° (producing increments of ~ 0.12°/projection). The exposure time for one projection was 1.4 msec, therefore the total scan time for each dentin specimen was about 35 minutes. The field of view was 100 µm.

CT Image Analyses

CT images were then imported into CTAn software version 1.13 (Bruker microCT, Belgium), which was used in assessing the X-ray linear attenuation coefficient (LAC, cm^{-1}) for each of the dentin specimens in each group. To assess LAC, a Region of Interest (ROI) was specified as having approximately 423 voxels (with each voxel having approximate volume of 51 nm x 51 nm x 51 nm). Two ROIs were specified for each CT image: one within the dentin tubule structure (i.e. 'tubular dentin') and between tubules (i.e. 'inter-tubular dentin'). An example demonstrating tubular ROIs is shown in Figure 4.

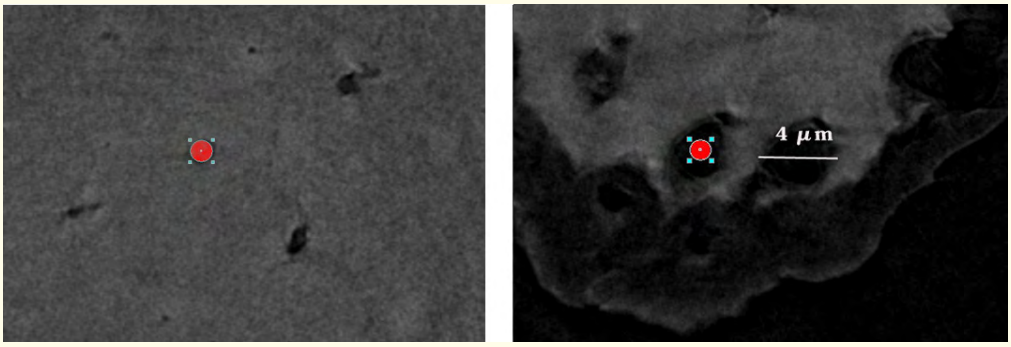

Figure 4: *Example ROIs (regions of interest) made on tubular dentin in the left and right CT images from specimens from groups S and A, respectively. Each ROI (denoted by red marker) was approximately 423 voxels (diameter of ~ 1.18 μm) and a 4 μm scale bar is shown for size comparison. Tubular dentin in sound dentin is a little smaller than the ROI.*

We note for the sound dentin specimens, tubule apertures were smaller than the ROI: thus, unavoidably, signal from inter-tubular and peritubular dentin is contributing to tubule profiling. With multiple scans of a specimen, the scanning of multiple specimens, and the high-flux character of the current X-ray CT setup, the sound dentin 'tubular' profiling represents an average over the tubular, inter-tubular and peritubular regions. For each ROI, increments of 51 nm into dentin resulted in 90 data points extending from the surface (51 nm) to 4,590 nm. Five iterations were made per specimen ROI, producing 450 data points per ROI. For the 5 specimens each in groups S, D, B and C, this amounted to 2,250 data points per ROI; for group A, one of the samples was excluded due to inadvertent movement error introduced during X-ray collection on the rotary stage, resulting in only 4 specimens with a total of 1,800 data points per ROI. Mean LACs were then determined for each ROI for each group.

Statistical Analyses on CT data

To obtain an approximate measure of statistical significance, statistics on LAC values were determined using the statistical package SAS-JMP (SAS Institute, USA) as follows. LAC values were grouped into nine 'test points' over every nine spatial increments, or 450 nm per ROI, and then averaged to construct a mean LAC value over a given distance. For example, LAC values grouped and averaged from 51 nm thru 459 nm were considered the 'first' statistical test point and were compared against other groups at this test point. This process was repeated for the remainder of the LAC values and produced a total 10 mean LAC values per ROI per group at depth points 51, 510, 1020, 1530, 2040, 2550, 3060, 3570, 4080 and 4590 nm. The mean LAC values corresponding to these ten depth points were then assessed for significance ($p < 0.05$) using the multiple comparison Tukey's HSD method. All data were normally distributed.

Field Emission Scanning Electron Microscopy (FE-SEM)

Dentin samples from each of the five groups were carefully selected for evaluation with a Zeiss Ultra 55 ultra-low voltage field-emission scanning electron microscope (Carl Zeiss Microscopy Co., Ltd., Germany). Samples were treated with osmium tetroxide (Neoc-STB, Meiwaforsis Co., Japan) to reduce electrical charging. Out-Lens SE2 (secondary electron) and In-Lens BSE (backscattered electron) detectors were used to collect scattered electrons operating at 1 kV and 200 pA. The aperture was fixed at 60 μm and high-resolution (1,000x

768 pixels) magnifications of 1,000x (for the Out-Lens SE2 detector) and 10,000x and 20,000x (for the In-Lens BSE detector) were used to image dentin surface from each of the five groups.

Samples were also analyzed for elemental composition using energy dispersive X-ray spectroscopy (EDX). An electron beam operating at 7 kV and 1.4 nA was focused on the sample under magnification of 2,000x. Emitted X-rays over a period of 20 minutes were collected with an EDS detector model NSS312E (Thermo Fisher Co., USA).

Focused-Ion Beam (FIB)

Representative dentin samples from groups D and A were then selected for cross-sectional evaluation. These cross-sections were etched using FIB (AURIGA, Carl Zeiss Microscopy Co., Ltd., Germany) with a Gallium (Ga) ion source. Samples were treated with Osmium tetroxide (Neoc-STB, Meiwaforsis Co., Japan) to reduce electrical charging of samples. Ga milling was performed at 30 kV and 4 nA. An Out-Lens SE2 detector collected scattered electrons operating at 1 kV and between 100 and 200 pA. Samples were transferred to the Ultra 55 for elemental analysis as described above.

3D Renderings from CT, FIB Images

Compositional-contrast information was obtained on the group D and A specimens described above using Energy Selective Backscattered (EsB) and Secondary Electrons Secondary Ions (SESI) detectors. These images were then imported into software for construction of 3D renderings. *In vivo* 5 software version 5.1 (Anatomage, USA) was used for 3D reconstruction of CT, EsB and SESI detector image files of FIB, and is commonly used as a visualization tool in the medical and dental sciences. Image files were converted to *In vivo* file format and rescaled accordingly to account for voxel/pixel size differences, as the native *In vivo* scale is in millimeters.

ATRAS version 4.5 (Fibics Co., Canada) and Amira version 5.4.2 FEI edition (Pro Medicus Ltd., Australia) software were used to construct 3D renderings from EsB and SESI image files. ATRAS 3D was used to construct 3D images from SEM images within the field of view (FOV). The resolution used was 13 nm per pixel, and the FOV was 2048 x 2048 pixels (26.6 µm x 26.6 µm). Amira software was used to construct images based on region of interest (ROI). The resolution was 13 nm per pixel, and the ROI was 1000 x 1000 pixels (13 µm x 13 µm).

Results

Digital Light Microscopy

The integrity of the dentin specimens was initially assessed using digital light microscopy. Representative bright field reflected light images of tapered dentin samples corresponding to each of the five groups (S, D, A, B and C) are shown in Figure 5 and reveal that the tapered dentin specimens have widths ranging between 50 and 70 µm along the directional axis at least 100 µm.

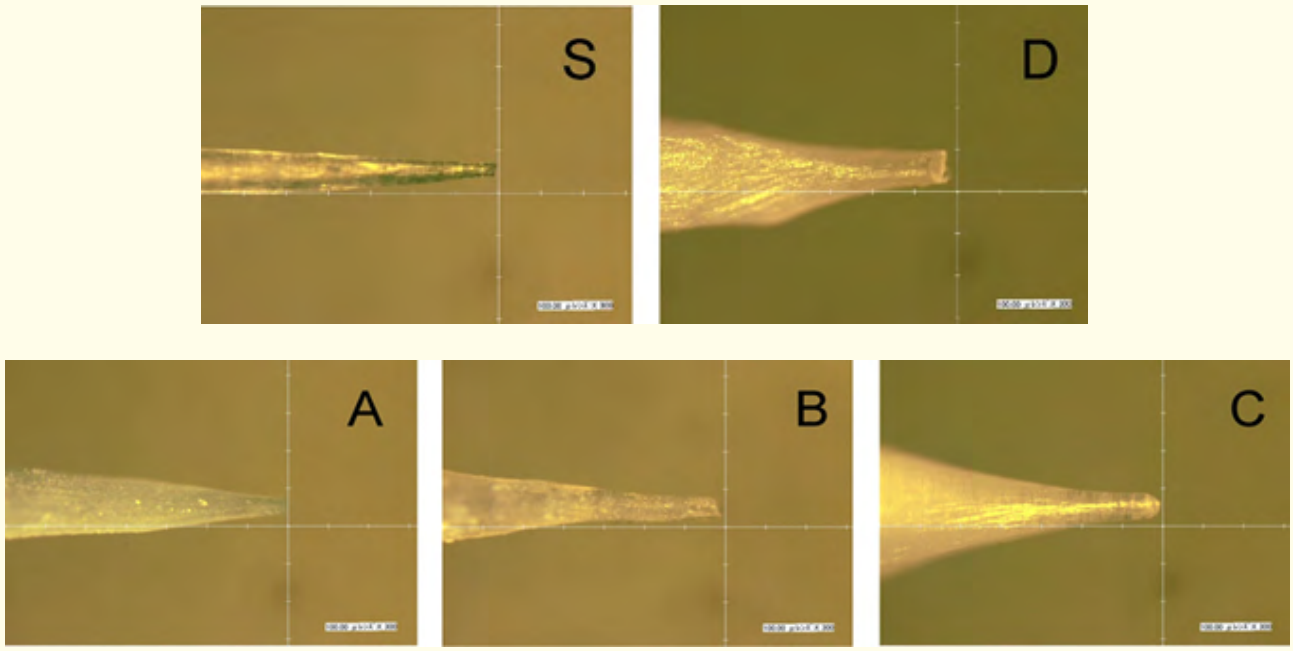

Figure 5: *Bright field reflected light images at 300x magnification of randomly selected dentin specimens from each of the five groups. Each image label corresponds to the respective treatment group. The white rectangular bar in each image represents 100 µm. The letters correspond to the following groups: sound dentin (S); demineralized dentin (D); and demineralized dentin treated with 0.2% NaF prophy paste (A), 1.1% NaF dentifrice (B); or, 5% NaF varnish (C).*

SR X-ray CT

Representative SR X-ray CT images for each of the five groups are shown in Figure 6. Each of the images contains four panels, with the lower right image a volume rendering based on the compilation of dentin cross-sectional projection images, three of which are shown as examples in each four-paneled image. Each of the three views (upper left panel: top view; and, upper right and lower left panels: side views) manifest vertical and horizontal scale bars extending to the limits of each of the panels, and were obtained using Anatomage in vivo software. The lower right panel reveals sound dentin specimen as relatively solid and smooth throughout, with intact tubules appearing as relatively dark, crack-like features in the three cross-sectional panel views. These features contrast with the demineralized specimen, which reveals porosity representative of bulk loss of mineral. Relative to sound dentin, the morphology appears less smooth and appears to manifest pronounced contouring as shown in the volume rendering panel (lower right image). Among the three treatment groups, the relative increase in porosity along with the presence of pronounced crevices indicate the loss of bulk mineral. Additionally, though the dentin cross-sections may appear quite dense (at least as dense as sound dentin), the contouring in the volume rendering panels for each of the treatments groups do not appear as smooth as that exhibited by sound dentin.

The mean empirical linear attenuation coefficients, for tubular and inter-tubular dentin as a function of dentin depth are shown in Figure 8a and 8b, respectively. With respect to sound dentin, the tubular LAC values demonstrate a gradual loss in mineral density deeper into dentin, while the inter-tubular regions maintain some constancy over the same length scale. The tubular LAC values reveal greater sensitivity to initial demineralization, where the loss of mineral density in inter-tubular regions extends down to about 2.5 µm, while

demineralization within the tubules extends beyond, reaching the limits of our experimental setup at depths around 4.5 μm. Similarly, the tubular regions demonstrate greater response to subsequent remineralization compared to inter-tubular regions. Within the inter-tubular region, the effects of the three fluoride treatments appear to increase the LAC values though these observations cannot readily discern differences among the treatment groups. However, the response of demineralized tubules appears sensitive to treatment, with the higher fluoride treatments of the dentifrice and varnish conferring larger LAC values. Though the treatment model used in this study was not optimized for statistical differences, modest analyses of these data were performed in order to garner a degree of how sensitive demineralized dentin was to treatment regimen.

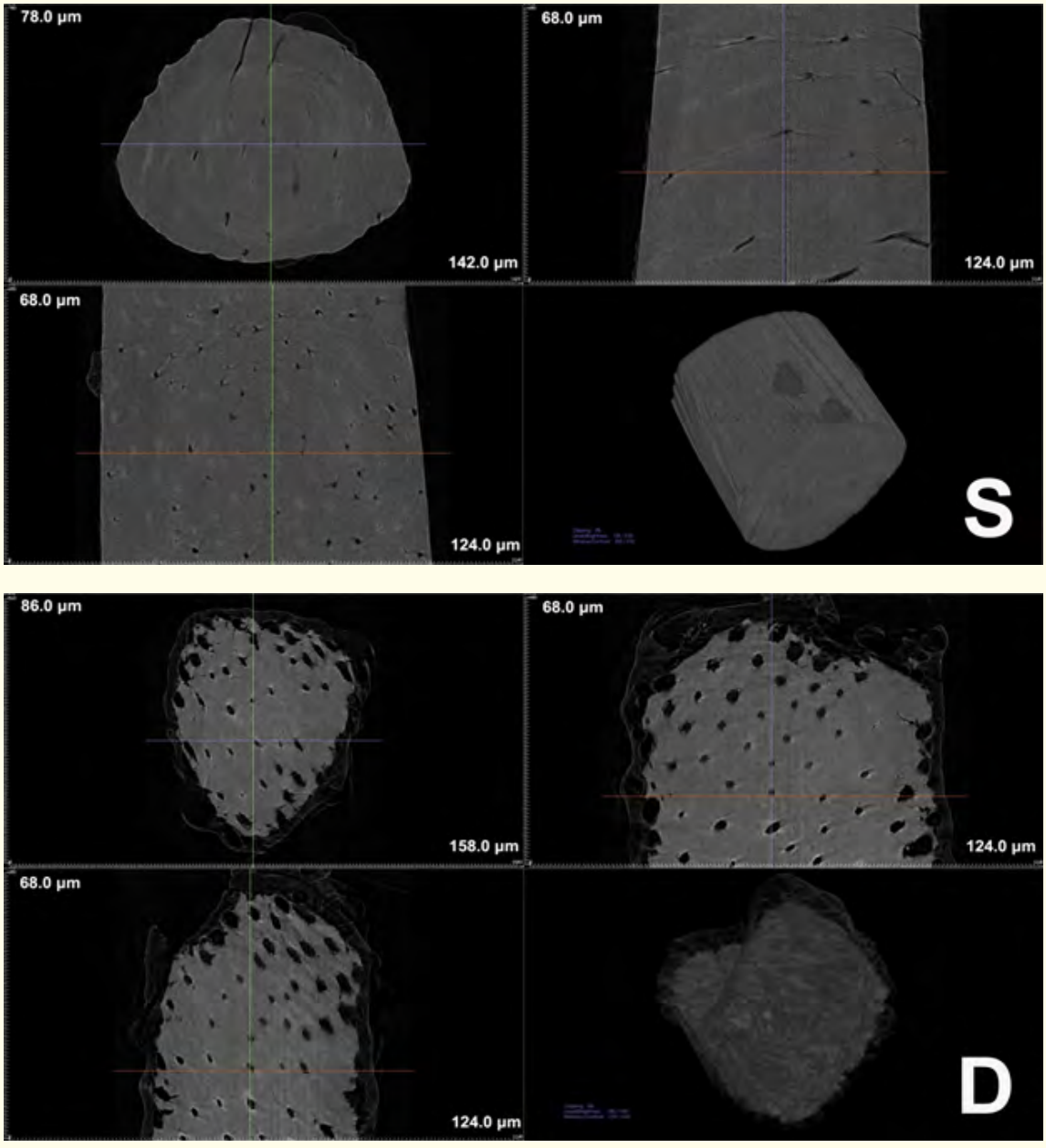

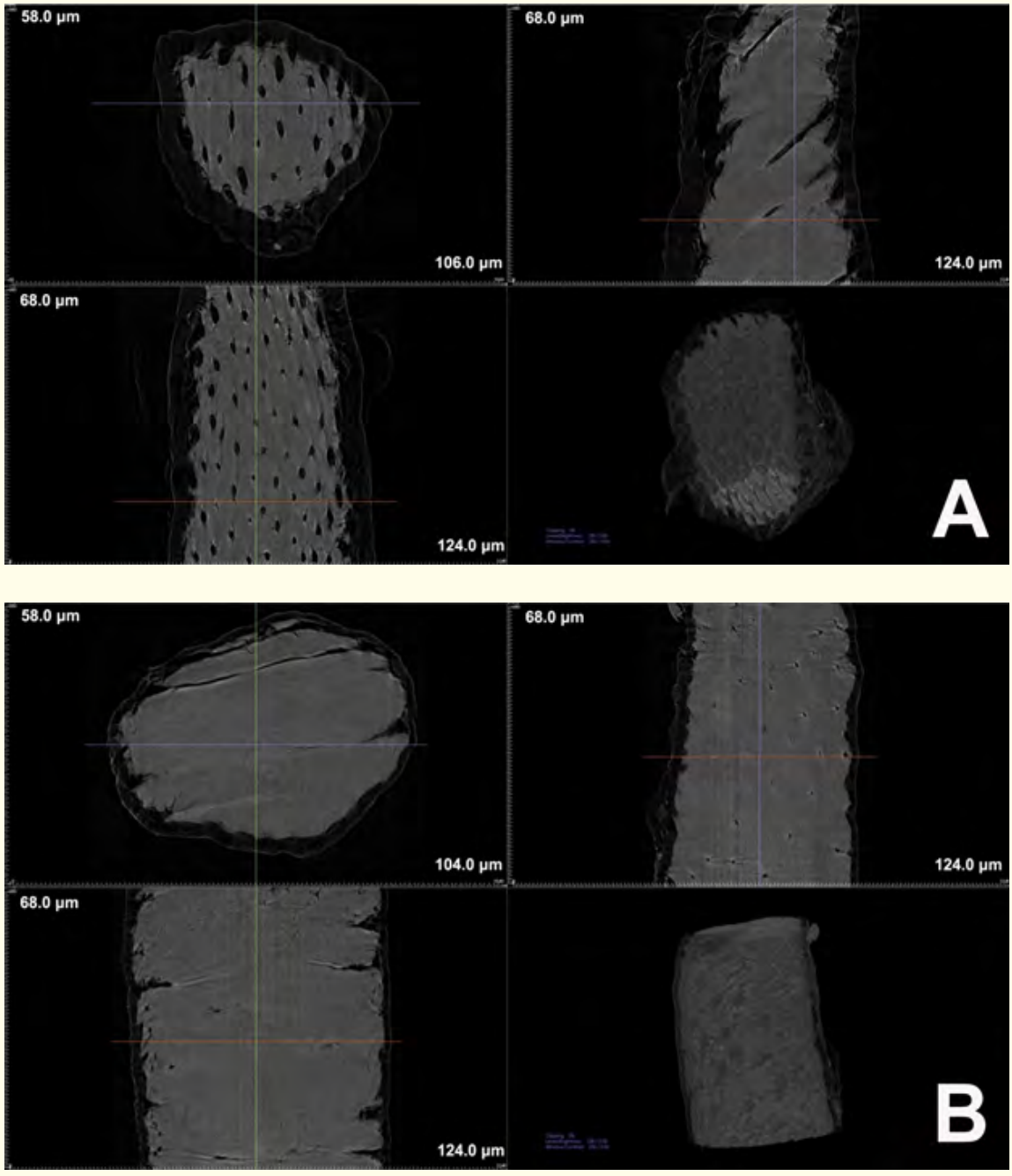
58.0 µm
106.0 µm
68.0 µm
124.0 µm
68.0 µm
124.0 µm
A
58.0 µm
104.0 µm
68.0 µm
124.0 µm
68.0 µm
124.0 µm
B

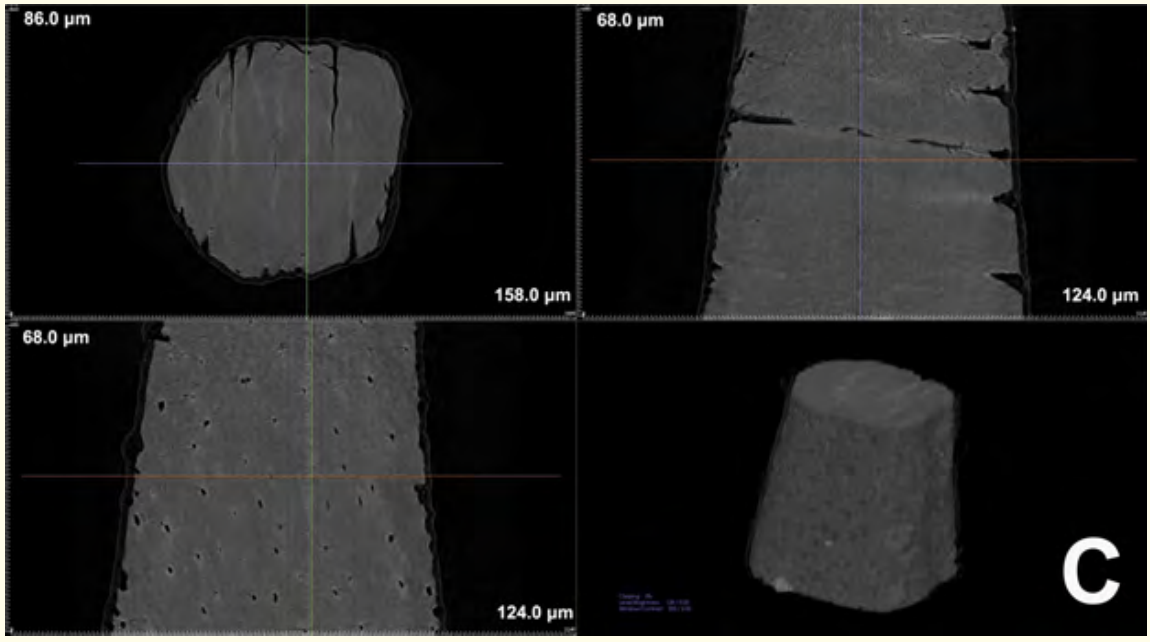

Figure 6: *Representative dentin slice cross-sections (upper left and right, and lower left) and volume rendering images (lower right) obtained from SR X-ray CT projection scans. Each of the three sectional views contains horizontal and vertical scales extending to the limits of each image (e.g. for the upper left panel in group S the horizontal and vertical scales are 142 µm and 58 µm, respectively. Each panel grouping labeled with the treatment group: sound dentin (S); demineralized dentin (D); and demineralized dentin treated with 0.2% NaF prophy paste (A), 1.1% NaF dentifrice (B); or, 5% NaF varnish (C). The volume rendering panel (lower right) reflects the field of view for the SR X-ray CT experiment.*

Using the approach described in the Methods section, statistics were determined for mean LAC values at depth points 51, 510, 1020, 1530, 2040, 2550, 3060, 3570, 4080 and 4590 nm for each ROI and each group. Prior to statistical analyses, the empirical relationship = $1.55 \cdot \mu_{LAC}$-1.05 was used in determining from experimental data collected from each of the five dentin groups [20]. The results are shown in Tables 2 and 3 for tubular and inter-tubular dentin, respectively. Statistical differences were readily observed among the groups for both tubular and inter-tubular ROIs. Notably, the relatively larger standard deviations for tubular LAC values relative to inter-tubular values indicate the averaging method used to compile the data may overestimate the LAC-distance relationship; though the treatment model and statistical methods were not optimized, statistical analyses are useful in quantitatively assessing the differences among the treatment groups. For tubular ROIs, statistical comparisons show group B conferred the greatest increase in LAC values among the fluoride-containing treatment groups, while the prophy paste conferred the least; for inter-tubular ROIs, group B and C conferred the greatest increases in LAC values 4.59 µm. The legend in the bottom figure corresponds to both histograms: sound dentin (S); demineralized dentin (D); and demineralized dentin treated with 0.2% NaF prophy paste (A), 1.1% NaF dentifrice (B); or, 5% NaF varnish (C).

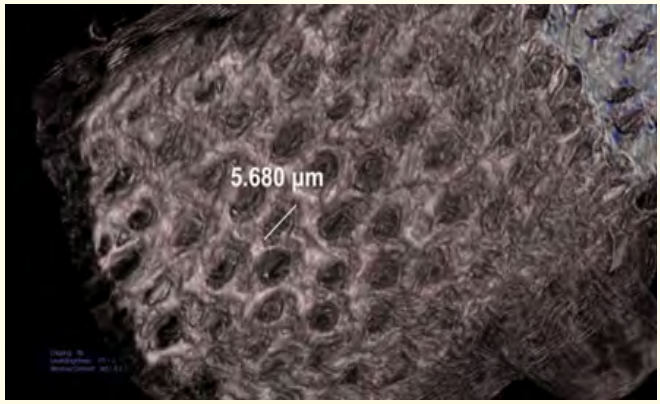

Figure 7: *Close-up view of the volume rendering image obtained from SR X-ray CT data. This image is from group A and the white scale bar spanning one patent tubule corresponds to 5.68 µm.*

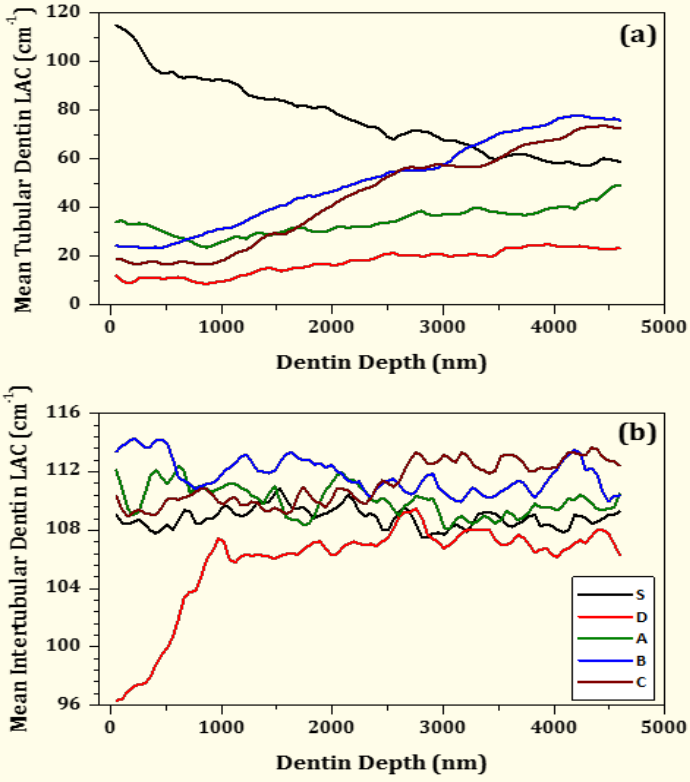

Figure 8: *Mean empirical linear attenuation constants for tubular (a) and intertubular (b) ROIs (~ 423 voxels) as a function of depth from the dentin surface down to 4.59 µm. The legend in the bottom figure corresponds to both histograms: sound dentin (S); demineralized dentin (D); and demineralized dentin treated with 0.2% NaF prophy paste (A), 1.1% NaF dentifrice (B); or, 5% NaF varnish (C).*

Depth (nm)	Group S	Group D	Group A	Group B	Group C
51	105.8 (17.7)[d]	10.7 (4.1)[a]	33.0 (8.2)[c]	23.9 (17.7)[b]	17.7 (5.8)[a,b]
510	93.7 (20.6)[c]	10.1 (5.8)[a]	26.2 (7.6)[b]	27.7 (16.1)[b]	17.2 (9.5)[a]
1020	87.7 (20.1)[d]	12.8 (9.8)[a]	28.3 (7.8)[b,c]	35.4 (14.2)[c]	24.1 (13.9)[b]
1530	82.0 (18.4)[d]	15.7 (13.0)[a]	30.8 (10.8)[b]	44.1 (21.1)[c]	34.4 (10.1)[b]
2040	74.4 (15.1)[d]	18.6 (12.2)[a]	32.6 (12.5)[b]	50.9 (26.5)[c]	47.4 (12.6)[c]
2550	70.1 (12.6)[d]	20.6 (12.2)[a]	36.8 (16.1)[b]	55.8 (28.0)[c]	56.5 (16.5)[c]
3060	64.0 (12.8)[c]	20.6 (13.0)[a]	38.5 (16.8)[b]	65.6 (29.1)[c]	57.7 (19.1)[c]
3570	60.5 (14.7)[c]	24.2 (12.5)[a]	38.3 (17.6)[b]	73.3 (31.2)[d]	66.0 (23.6)[c,d]
4080	58.7 (17.0)[c]	23.7 (11.3)[a]	43.2 (22.5)[b]	77.1 (29.7)[d]	72.3 (22.9)[c,d]
4590	59.0 (16.6)[a,b]	23.4 (12.0)[a]	49.2 (26.6)[b,c]	76.0 (32.5)[c]	72.7 (26.2)[c]

Table 2: *Statistical comparisons of tubular mean (std. dev.) LAC values (μ) for ROIs foreach of the five dentin groups at each. Subscripts indicate statistical differences (p <0.05), where a < b < c < d.*

Depth (nm)	Group S	Group D	Group A	Group B	Group C
51	108.4 (6.0)[b]	97.6 (3.7)[a]	110.8 (4.2)[b]	113.9 (7.0)[c]	109.4 (2.5)[b]
510	108.8 (6.4)b	103.8 (4.5)[a]	111.2 (3.6)[b]	111.7 (6.5)[c]	110.4 (2.0)[b,c]
1020	109.6 (5.4)[b]	106.3 (3.4)[a]	110.7 (2.4)[b,c]	112.4 (5.4)[c]	109.8 (3.3)[b]
1530	109.5 (3.8)[b]	106.6 (4.3)[a]	109.4 (2.0)[b]	112.8 (3.5)[c]	109.9 (4.0)[b]
2040	109.2 (3.5)[b]	107.0 (2.8)[a]	110.9 (2.5)[b]	111.2 (4.3)[b]	110.6 (4.8)[b]
2550	108.3 (3.5)[a]	108.3 (2.6)[a]	109.6 (2.8)[a,b]	111.1 (4.9)[b]	112.5 (4.1)[b,c]
3060	108.7 (3.0)[a,b]	107.7 (2.6)[a]	108.7 (3.0)[a,b]	110.4 (4.6)[b]	112.6 (4.2)[c]
3570	108.5 (2.6)[a,b]	107.9 (2.7)[a]	109.3 (2.4)[b,c]	111.2 (4.3)[c,d]	112.5 (5.2)[d]
4080	108.7 (3.0)[a,b]	107.3 (3.0)[a]	109.8 (3.0)[b]	112.0 (3.3)[c]	113.2 (4.7)[c]
4590	109.3 (3.0)[a]	106.3 (2.4)[a]	110.5 (4.0)[a]	110.4 (4.8)[a]	112.5 (4.1)[a]

Table 3: *Statistical Comparison of inter-tubular mean (std. dev.) LAC values (μ) for ROIs for each of the five dentin groups at each. Subscripts indicate statistical differences (p < 0.05), where a < b < c < d.*

To obtain information on the approximate mineral concentrations in tubular and intertubular dentin for each of the five groups, the following relationship was used [20].

$$\mu = \rho \sum_i w_i \tau_i(E) = \rho w_{Collagen} \tau_{Collagen} + \rho w_{H_2O} \tau_{H_2O} + \rho w_{HAP} \tau_{HAP}$$

where μ is calculated from the experimentally determined linear attenuation coefficient (μ_{LAC}) of the material, ρ is the density of the material, w_i is the weight fraction of component i in the material, and $\tau_i(E)$ is the mass attenuation coefficient (MAC) of the component i at X-ray energy E. For dentin, we assumed the three largest components by weight would be Type I collagen, water and hydroxyapatite (HAP) mineral. Using the relationship $C_i = \rho w_i$, rearrangement of equation (1) for the HAP mineral concentration in dentin (C_{HAP}) yields.

$$C_{HAP} = \frac{\mu - \rho w_{Collagen}\,\tau_{Collagen} - \rho w_{H_2O}\tau_{H_2O}}{\tau_{HAP}}$$

As noted above, the empirical relationship $\mu = 1.55 \cdot \mu_{LAC} - 1.05$ was used in determining μ from experimental μ_{LAC} data collected from each of the five dentin groups. Due to the microscope optics used in collecting experimental data, μ_{LAC} is approximately 90% of the calculated value μ [20]. We used the density of dentin (ρ = 2.29 g·cm^{-3}) determined by averaging densities of human molar dentin previously reported [36]. We used the empirical weight fractions of 22% and 13% for collagen and water, respectively [37,38]. The MACs for collagen (Type I, $C_{12}H_{24}O_4N_3$ [39]), water (H_2O) and HAP ($Ca_6P_6O_26H_2$) in dentin ($\tau_{Collagen}$, τ_{H_2O}, and τ_{HAP}) at 8 keV are, respectively, 6.31 cm^2·g^{-1}, 10.37 cm^2·g^{-1} and 87.86 cm^2·g^{-1} [40]. These parameters were used in determining C_{HAP} for both tubular and intertubular dentin as a function of dentin depth as shown in Figure 9a and 9b, respectively.

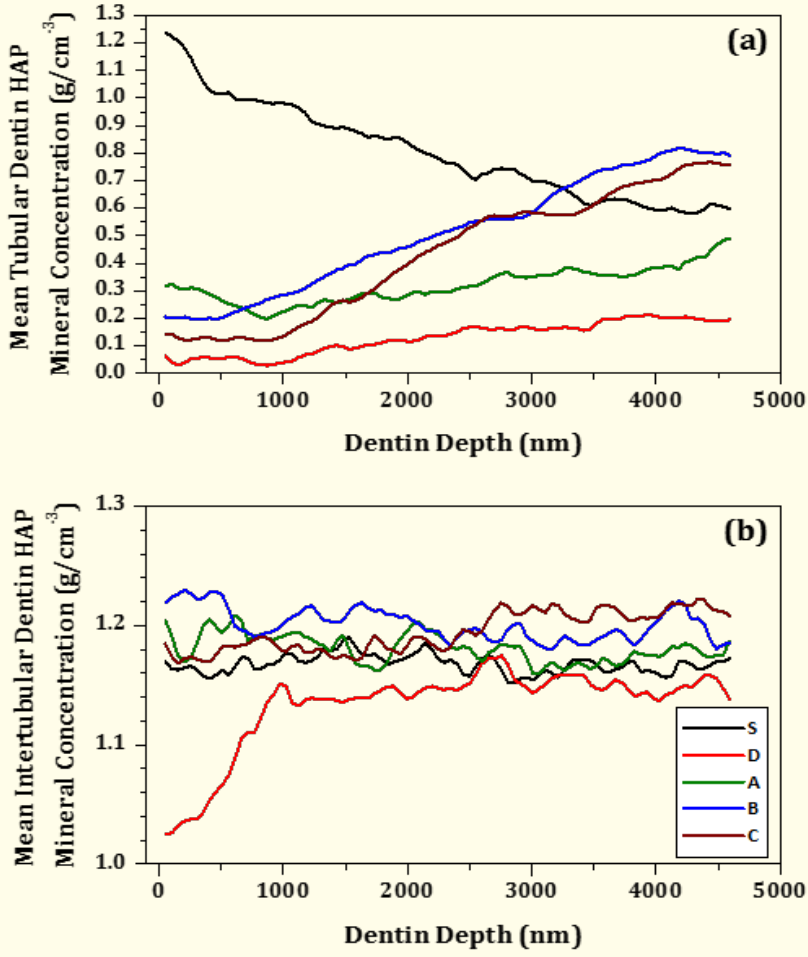

Figure 9: *Mean mineral concentration for tubular (a) and intertubular (b) ROIs (~ 423 voxels) as a function of depth from the dentin surface down to 4.59 µm. The legend in the bottom figure corresponds to both histograms: sound dentin (S); demineralized dentin (D); and demineralized dentin treated with 0.2% NaF prophy paste (A), 1.1% NaF dentifrice (B); or, 5% NaF varnish (C).*

FE-SEM

Representative FE-SEM images of the five enamel groups at 1,000x, 10,000x and 20,000x magnifications are compiled in Figures 10 thru 12, respectively. At low magnification (1,000x in Figure 10), sound dentin appears relatively smooth and non-porous, while demineralized dentin manifests a rougher texture concomitant with an abundance of microscopic openings. The fluoride treatments (prophy paste, dentifrice and varnish) all appear to confer a degree of mineralization and/or tubule occlusion on each respective demineralized substrate as the porosity and tubules openings appear diminished relative to the demineralized dentin control. Among the fluoride treatments, group A specimens appear to remineralize but not as well as extensively as groups B and C. Evidence of a mineralizing effect for group B specimens (e.g. Figures 10 and 11) can be noted in the wave-like features that appear to have been created on the outer surfaces of the substrate. For the varnish group C, in addition to remineralization effects, hints of undissolved resin appear to on the specimen (as shown in Figure 10), and support the difficulty in completely removing the expertly applied varnish treatment.

At higher magnifications (10,000x and 20,000x in Figures 11 and 12, respectively), morphological details reveal more information. The bulk loss of mineral during demineralization erodes mineral within the tubules as well as within the intertubular region as show in group D images. Treatments with the three different fluoride therapies revealed narrowing of tubule openings relative to the demineralized dentin control. Specimens treated with group A were exposed to the prophy paste formulation, which contains silica microspheres (1 µm to 1.5 µm in diameter) for the express purpose of tubule occlusion, such as that observed in Figures 11 and 12. Treatment with groups B and C narrowed the tubule apertures and produced textural variations, effects of which are indicative of mineralization.

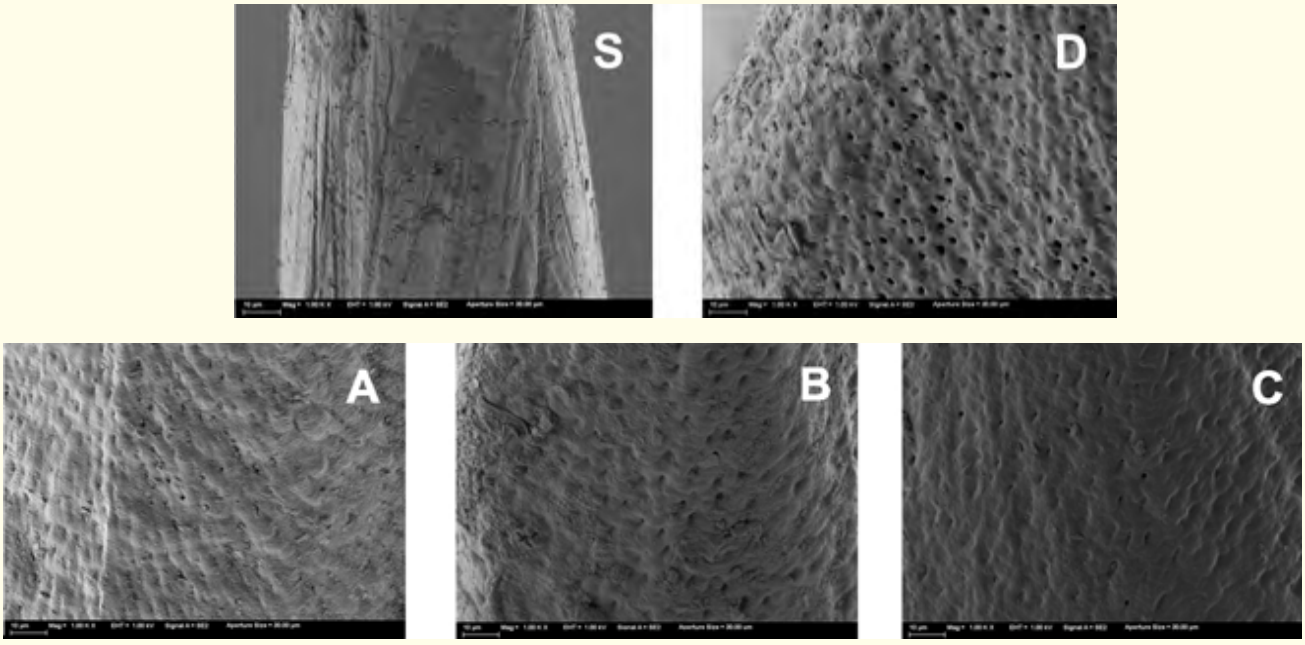

Figure 10: *FE-SEM images (1,000x magnification) of randomly selected dentin specimens from each of the five groups. For all images the white scale bar (bottom left) corresponds to 10 µm. The letters correspond to the following groups: sound dentin (S); demineralized dentin (D); and demineralized dentin treated with 0.2% NaF prophy paste (A), 1.1% NaF dentifrice (B); or, 5% NaF varnish (C).*

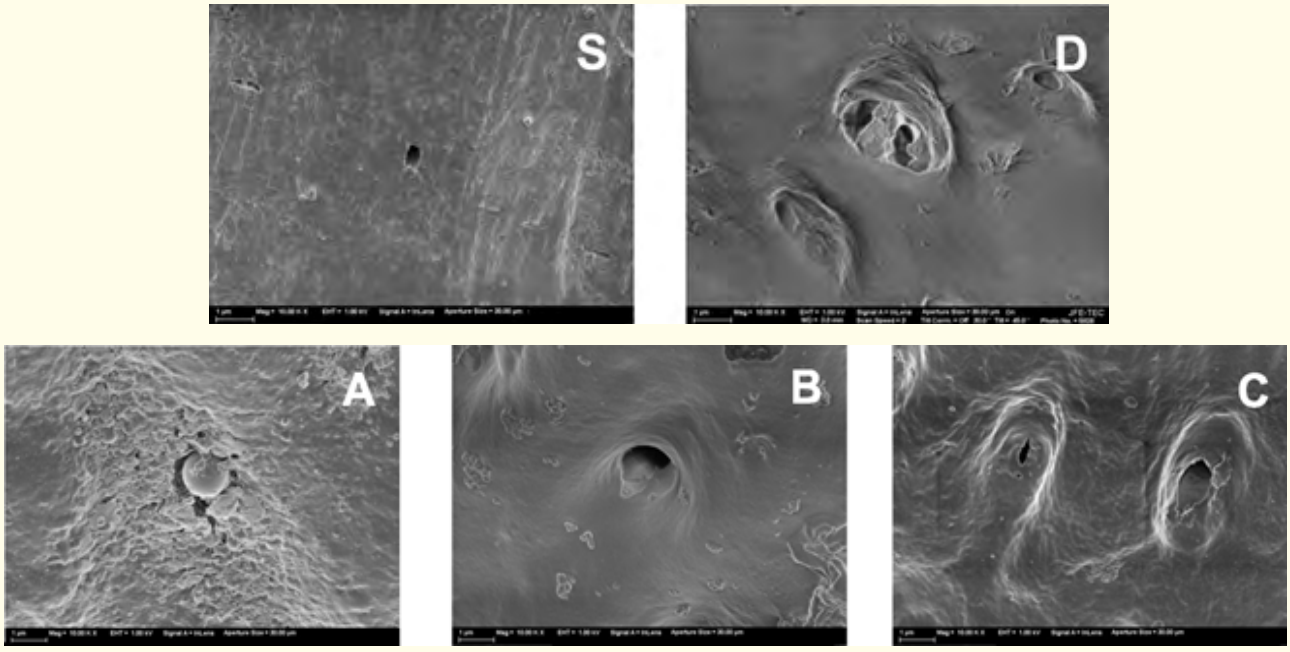

Figure 11: *FE-SEM images (10,000x magnification) of randomly selected dentin specimens from each of the five groups. For all images the white scale bar (bottom left) corresponds to 1 µm. The letters correspond to the following groups: sound dentin (S); demineralized dentin (D); and demineralized dentin treated with 0.2% NaF prophy paste (A), 1.1% NaF dentifrice (B); or, 5% NaF varnish (C).*

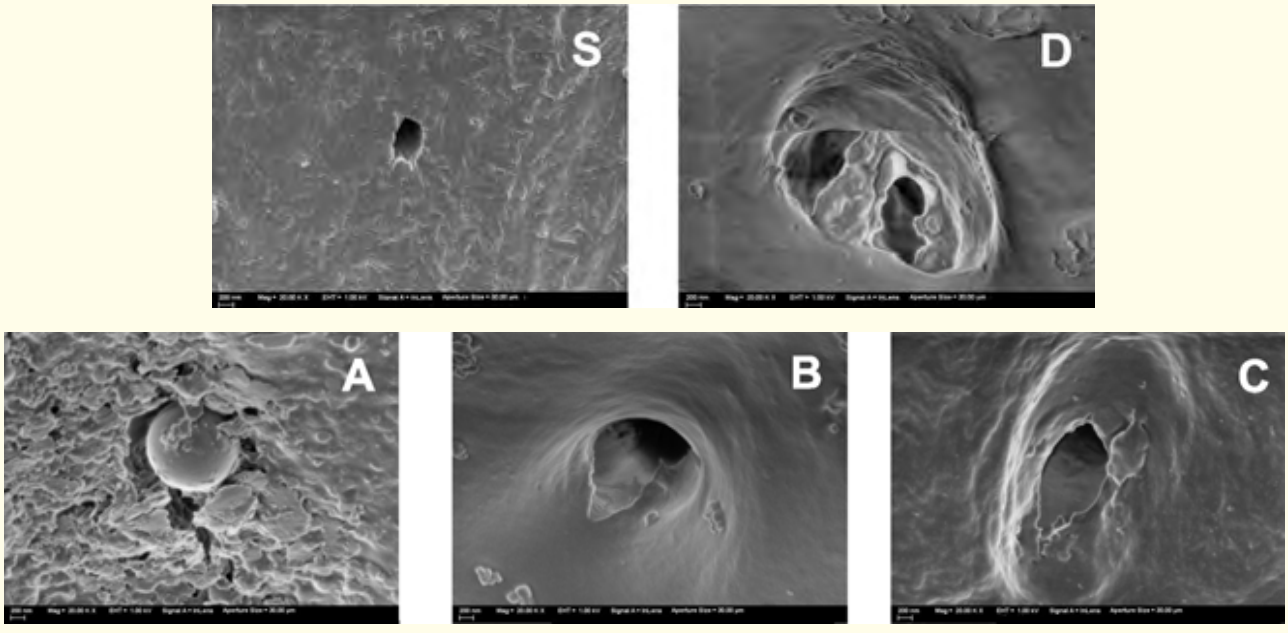

Figure 12: *FE-SEM images (20,000x magnification) of randomly selected dentin specimens from each of the five groups. For all images the white scale bar (bottom left) corresponds to 200 nm. The letters correspond to the following groups: sound dentin (S); demineralized dentin (D); and demineralized dentin treated with 0.2% NaF prophy paste (A), 1.1% NaF dentifrice (B); or, 5% NaF varnish (C).*

Randomly selected specimens from each group were also assessed for elemental composition via EDX spectroscopy. Additionally, two samples from groups D and A were also selected for FIB via Ga milling: in this case, the resultant cross-sections were also mapped for composition. A compilation of the elemental mapping is shown in Figure 13. The maps shown include the following elements: carbon, nitrogen, oxygen, calcium, phosphorous, fluorine, magnesium, sodium and silicon. Additionally, minor detection of elements aluminum, chlorine and sulfur were also detected but because the concentration was very low and not ubiquitous to all of the groups these are not shown for purposes of conciseness. Additionally, a baseline 'grey' FE-SEM image is shown in the top row for all groups. For the Ga milled samples, a thick band (~ 2.5 μm) is observed and represents embedded gallium ions during the milling procedure.

The maps for sound dentin reveal Ca, P, Mg, Na and O are the dominant elemental components. Notably, sound dentin also contains a moderate level of fluorine. Upon demineralization, the bulk loss of each of these elements renders the C and N environments as the remaining abundant species, with fluorine also remaining in modest concentration. The demineralized dentin substrates also reveal a dearth of Ca, P and Mg as shown in the top-view elemental maps; however, these elemental absences do not extend throughout the body of the demineralized substrate, as the cross-sectional maps (e.g. the second to last column on the right) indicate relative abundance of Ca, P and O about 2.5 μm down from the outer dentin surface. The cross-sectional maps also reveal regions devoid of mineral, and this may correspond to demineralized tubules. These observations are mirrored in the demineralized dentin treated with group A. As in the demineralized control, fluorine remains one of the more concentrated elements in this specimen, and its presence is also reflected in relative abundance of Na. Both the surface and cross-sectional maps reveal the presence of Si and O 'dots', indicating deposition of silica microspheres into tubules as observed in the grey-scale image. Demineralized dentin treated with group B results in apparent silicon-rich particle depositions. These depositions also appear in the grey-scale image and overlap regions found in oxygen mapping, and therefore are likely a form of silica. Additionally, modest increases in Ca and P were found while those of C and N remained comparable to demineralized dentin. This situation is opposite for group C, where relatively large C and N signals indicate a relative abundance of organic material.

FIB 3D Renderings

A collection of EsB images from a group A specimen cross-section are shown in Figure 14. These images were subsequently imported into *In vivo* 5 software, where volume renderings were generated as shown in Figure 15. The white bands in Figure 14 reflect the incorporation of gallium during the Ga milling process. Additionally, patent tubules are readily observed, with openings readily visible in both EsB and volume rending figures. Notably, the presence of at least one spherical body is visible in both figures. The upper right-hand image in Figure 15 reflects the use of the 'soft tissue mode' of the Invivo software, and depicts the approximate size of one of these occluding bodies (~ 1 μm in diameter). With support from FIB cross-sectional elemental mapping in Figure 13, the spherical body likely derives from the silica microspheres present in the prophy paste formulation.

A comparison of SESI images on specimen cross-sections from groups D and A is shown in Figure 16. *In vivo* software was again used to generate volume renderings. The 3D rendering reveals relatively larger tubule openings for the demineralized group (D) and supports 2D FE-SEM imaging. With respect to the 3D rendering for the group A cross-section, in addition to relatively smaller tubule openings, the presence of additional materials are also observed, and could be related to mineralization and/or depositions of prophy paste ingredients (e.g. an abrasive).

Finally, a compositional-contrast comparison between EsB and SESI for the group A cross-section is shown in Figure 17. These figures were rendering using ATRAS 3D and Amira software, and compare favorably to the Invivo rendering in Figure 15. Between the two detectors, the EsB detector may provide somewhat greater resolution around tubule opening, although both detectors collected similar compositional-contrast data. The two detection methods do not appear to capture new information, although the contrast flexibility certainly offers visibility options as desired.

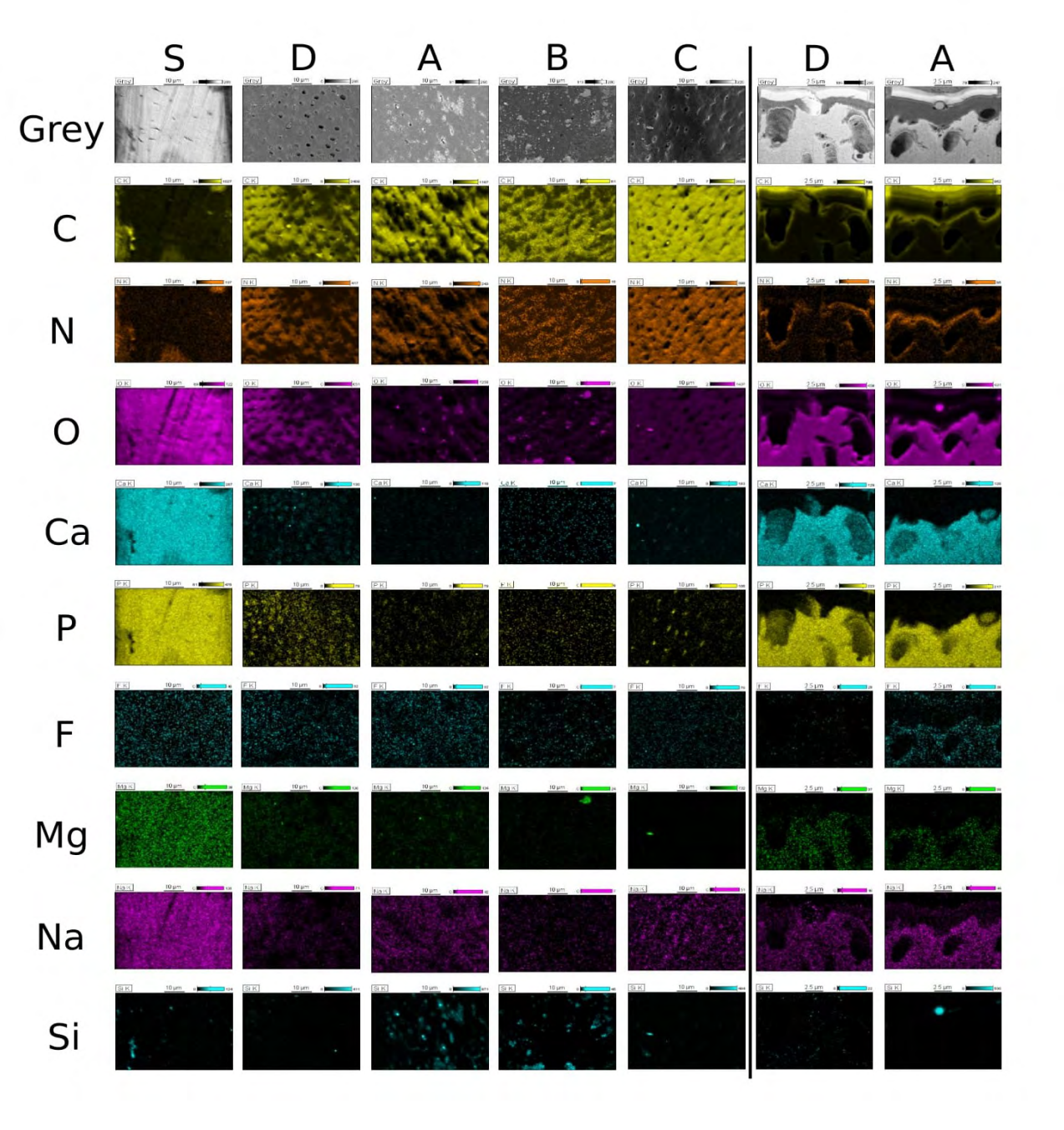

Figure 13: *EDX elemental mapping of randomly selected dentin specimens from each group obtained by FE-SEM. A solid vertical bar separates the collection of elemental maps as follows. The first five columns ('S' thru 'C') contain maps generated from the outer dentin surfaces (2,000x magnification). The scale bars shown at the center above each of these images is 10 µm. The last two columns on the right ('D' and 'A') represent mapping from dentin cross-sections obtained from FIB Ga milling (7,000x magnification). The scale bars shown at the center above each of these images is 2.5 µm. The letters correspond to the following groups: sound dentin (S); demineralized dentin (D); and demineralized dentin treated with 0.2% NaF prophy paste (A), 1.1% NaF dentifrice (B); or, 5% NaF varnish (C).*

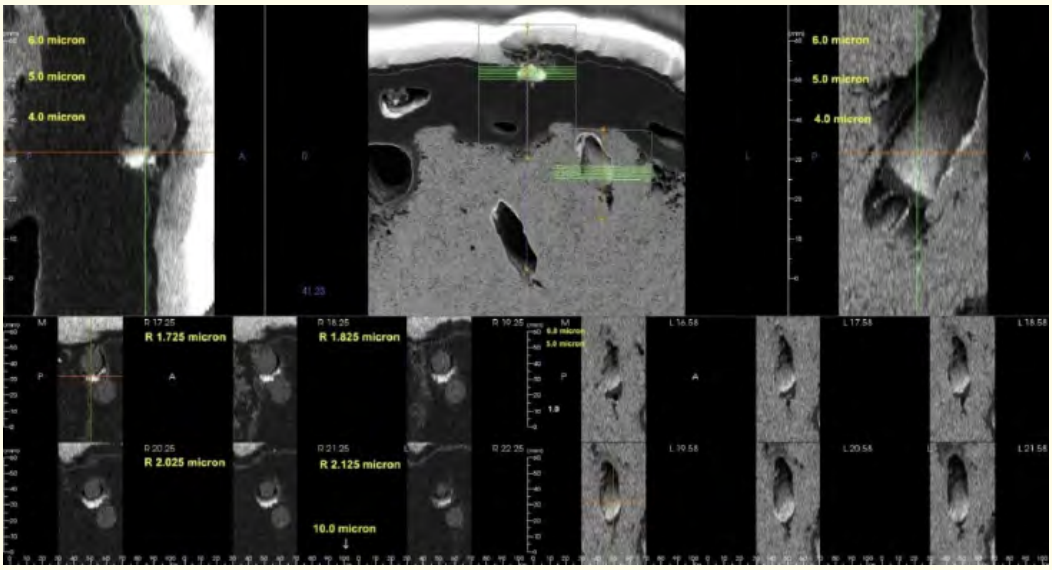

Figure 14: *Collection of EsB detector images collected via FIB on a group A specimen cross-section. These images were imported into Invivo 5 software, which then produced the volume rending image in Figure 15.*

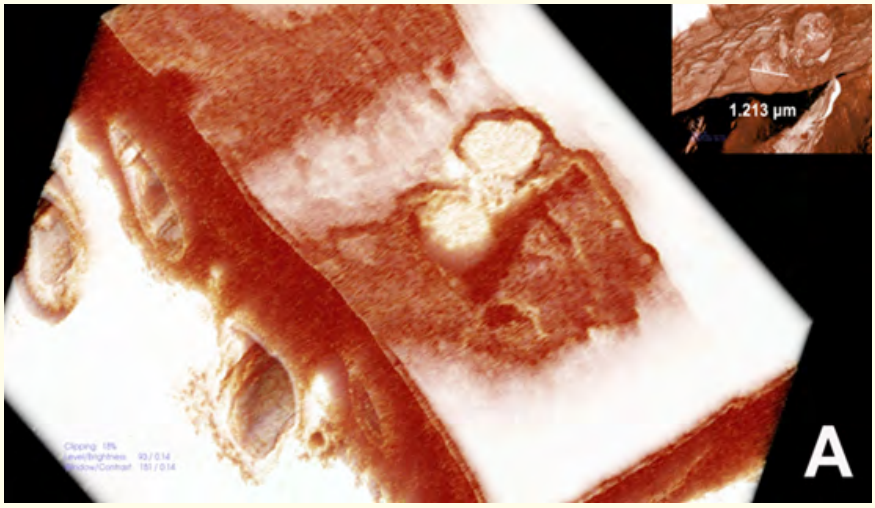

Figure 15: *Example 3D volume rendering image of a group A specimen based on multiple EsB images of specimen cross-sections obtained via FIB. Invivo 5 software was used to construct the main image, along with the contrast inversion (or, 'soft tissue mode') of the main image, which is shown in the upper right-hand corner. The contrast inversion image includes a white scale bar denoting 1.213 µm.*

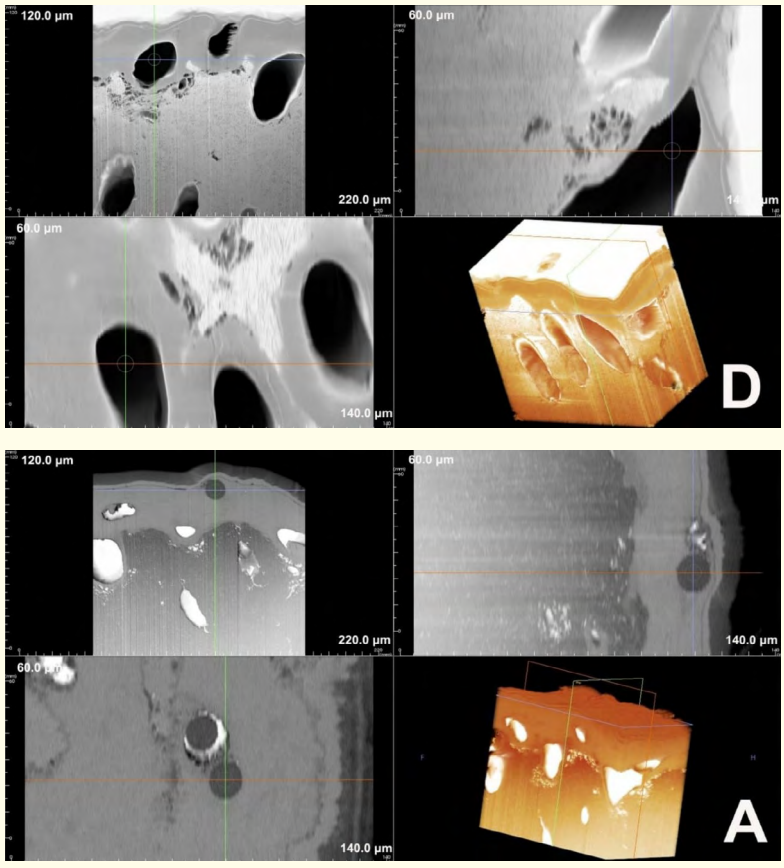

Figure 16: *Example of cross-sectional SESI and volume rendering images (lower right panel in each figure) for specimens from groups D and A generated from Invivo 5 software. The letters correspond to demineralized dentin (D) and demineralized dentin treated with 0.2% NaF prophy paste (A). The lower right panel of group A is a contrast inversion representation.*

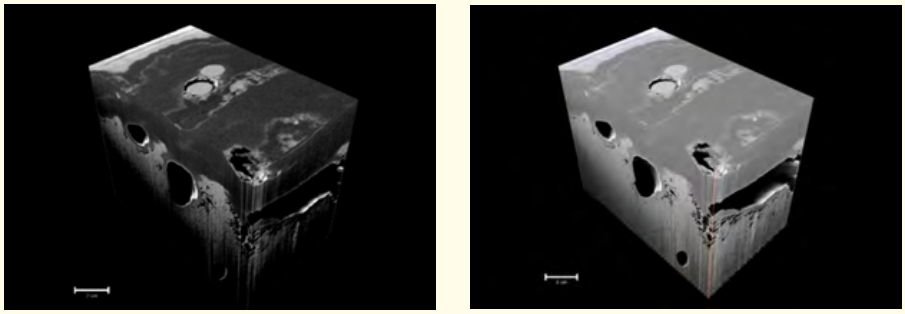

Figure 17: *Examples of composition-contrast volume renderings for the group A specimen cross-section. ATRAS 3D and Amira software were used to reconstruct 3D representations from EsB (left) and SESI (right) detector image files. White scale bar in both renderings corresponds to 2 µm.*

Discussion

X-ray CT offers numerous benefits in the evaluation of materials. Prime features of these experiments include the ability to generate non-destructive 3-D information on the internal structure of a material, especially 'soft' biological tissues such as dentin. Information gleaned from CT data include morphology, geometry and mineral concentrations at the micron scale, which can be readily applied, for example, to generate comparisons between sound and carious teeth or evaluate caries excavating methods [13-15]. With advances in experimental apparatus, such comparisons are supported with quantitative results [20,22].

In the present study, marked contrasts in mineral density, elemental composition and substrate morphology were observed between sound and demineralized tubular and intertubular dentin. For instance, tubular morphology changed considerably upon demineralization, where loss of crystalline structure resulted in wider and more irregular tubule openings. But two prominent findings in this research are a) the ability to distinguish between two dentin environments, and b) the ability to track the tubular region as a function of depth using SR X-ray CT; in fact, this study is among the few studies, if not the first study, to achieve such non-destructive empirical insight. While polychromatic sources of X-rays are typically used to collect conventional CT data, we utilized a high-flux, monochromatic source that enabled straightforward quantification of LAC values [18-23]. These LAC values were then used to estimate mean mineral concentrations for a range of dentin specimens. Importantly, our CT experiment incorporated innovative microscopic optics that facilitated data collection at submicron resolutions, enabling distinction between tubular and intertubular LAC values [20,22].

Furthermore, these resolutions allowed us to estimate mineral concentrations within dentin tubules as well as in the intertubular regions. Our analyses yielded mean (SD) intertubular mineral concentrations of ~ 1.16 (0.05) $g \cdot cm^{-3}$ over the depth of dentin (~ 4.59 μm) for sound dentin. In contrast, tubular mineral concentrations of sound dentin diminished almost linearly (R2 ~ 0.97 ± 0.04) from ~ 1.22 (0.15) $g \cdot cm^{-3}$ at the tubule opening to ~ 0.6 (0.18) $g \cdot cm^{-3}$ over the course of the dentin. We note the contributions of 'tubular' signal for sound dentin necessarily include intertubular, peritubular and tubular signal, but for the sake of discussion and simplicity we discuss this region as 'tubular'. This gradual decrease in mineral concentration indicates sound dentin tubules are comprised of multiple phases, and support the existence of other compositional phases known to exist within tubule structure, including ions, water-based fluids, and the presence of biologically active agents (including odontoblasts) [3,4,41]. These possibilities then bear on dentin permeability and biological signaling [1-4,6,41]. Until now, this non-destructive snapshot of natural HAP mineral declination as a function of dentin depth has not been previously observed. While other experimental methodologies might be suggested to probe such distinctions, SR X-ray CT is uniquely positioned by virtue of its non-destructive handling of specimens (compared to TEM, SEM, permeability studies etc). However, this X-ray tool does suffer drawbacks, including access to sophisticated equipment as well as the inherent limitation of X-rays in detection of radiopaque materials. Nevertheless, these results underline the importance of SR X-ray CT methodology and the need for further research elucidating the nature of the material phases existing within the tubule structures. We note our estimation of sound dentin mineral concentration is similar to those obtained by other CT investigations (~ 1.4 $g \cdot cm^{-3}$) [13,14]. Possible differences in estimated mineral concentration likely arise from estimations of dentin composition and experimental errors (including error introduced due to microscope optics in our study [20] as well as errors unavoidably introduced in the use of polychromatic X-rays in the other studies [13-16]), along with differences in region of interest (ROI) resolutions and dentin specimen source and preparation.

With respect to demineralized dentin obtained using dilute citric acid in a short-term exposure model, mean (SD) mineral concentrations within the dentin tubule remained near 0.15 (0.18) $g \cdot cm^{-3}$ over the depth of dentin (~ 4.59 μm); in contrast, the mean (SD) mineral concentration in the intertubular region was relatively higher at the tubule opening 1.02 (0.05) $g \cdot cm^{-3}$ and increased linearly (R2 ~ 0.98 ± 0.00) to ~ 1 μm, where it leveled off at approximately 1.15 (0.06) $g \cdot cm^{-3}$. Though we utilized an erosive challenge that principally targeted calcium phosphate mineral [42], these values span the calculations performed on carious dentin by other CT studies (between ~ 0.30 and 0.43 $g \cdot cm^{-3}$) [13,14]. The approximate order of magnitude difference between the two dentin regions demonstrate the compositional sensitivity of tubules. This observation underlines the importance of the collagen framework in dentin structure and confirms the multi-component composition within the tubules [1-5,43].

The trend in tubule mineral concentration suggests there are at least two mechanisms provided by the prophy paste in this short-term exposure model. Within the first 900 nm, a gradual decrease in mineral concentration is observed, at which point the mineral profile begins to increase, similar to the other fluoride groups. The apparent reduction in mineral concentration may be due in part to the inability of the X-ray experiment to resolve the radiolucent silica microspheres, which may affect LAC values; alternately, the occluding action of silica microspheres and/or other undissolved ingredients from the prophy paste at the dentin surface might function as seeds for ensuing mineralization, which would contribute to increases in apparent mineral concentration. Regardless, the effect appears to be limited around 900 nm, whereby a gradual and positive trend is observed, and probably is a combination of pre-existing undissolved mineral (since the slope is similar to the demineralized dentin control group) along with newly formed mineral permeating into the tubules. The fact that the trend is lower than those of the dentifrice and varnish groups around 1.5 μm indicates the prophy paste formulation has limited subsurface action. These limits may be due to occluding action originating near tubule openings. The primary reason for using the prophy paste in this study is to probe whether the formulation could deposit silica microspheres into patent tubules. Although its radiolucency thwarted detection with SR X-ray CT, detection via electrons and ions provided ample visibility of its ability to occlude tubules. Though additional studies may be warranted, these results suggest the formulation may provide potential hypersensitivity benefits. Importantly, the inclusion of silica microspheres appears to resist modest acid challenges as used in the present model. These observations are important as it supports the perspective of physically blocking patent tubules as a method to relieve dentinal hypersensitivity [1-4,6,41].

To achieve lasting remineralization benefits, it is advisable to use topical modalities, including fluoride dentifrices and varnishes [44]. As shown with elemental mapping, treatment with the dentifrice produced some silicon-rich depositions likely sourced from the silica abrasive [45]. The elemental mapping also revealed evidence of modest calcium and phosphorous-based mineralization at the dentin surface, that in turn maintained a diminished signal response from both carbon and nitrogen. SR X-ray CT results demonstrate the dentifrice provided both tubular and intertubular remineralization benefits, with a greater influence on the former region extending at least 4 μm into the tubular structures. Notably, there appeared to be an inductive effect within the first 500 nm, whereby increases in mineral concentration then proceeded more dramatically throughout the remaining depth of study. The inductive response may be due to an accumulation of a critical amount of mineral and/or mixed phase composition (e.g. including organic material) necessary to stabilize the initially demineralized tubule environment. Because the dentifrice delivers acid-resistant mineral [21,25-29,35,45], once a stabilizing 'plug' is achieved [3,6], then thermodynamic conditions drive secondary processes, such as mineral permeation. When coupled with previous studies on acid-resistant mineralization delivered from the fluoride plus functionalized TCP combination [21,25-29,35,45], these CT data suggest remineralized dentin becomes stronger than the original dentin state by virtue of an increase in the concentration of apatite-like mineral. A separate study evaluating the effect of this dentifrice on subsurface enamel lesions demonstrated the formation of numerous nanometer-sized apatite-like clusters within the demineralized structure [35]. Therefore, we believe a similar effect has promoted the relatively deep penetration of newly formed mineral. With the benefit of empirical data, future studies could probe the subsurface elemental composition using FIB. Still, the present results demonstrate the ability the fluoride dentifrice to confer substantial mineralization effects. We note that despite tubular increases in mineral concentration, tubule occlusion was not necessarily observed. Clinical studies have reported on relief of dentinal hypersensitivity from dentifrices containing fluoride plus functionalized TCP (e.g. Clinpro™ Tooth Crème, Clinpro™ 5000), despite the absence of robust tubule occlusion [46,47]. Therefore, the absence of obvious tubule occlusion suggests another mechanism may be contributing to *in vivo* relief of dentinal hypersensitivity [2,4]. We speculate that the mechanism likely involves an equilibrium of newly formed apatite-like mineral phases [35] intermingled with biological and organic-rich fluid phases [3], but such details are reserved for future study.

Because the varnish is a water-free, slow-dissolution system, it is possible that remnants of the varnish may have remained on the delicate dentin surface and may have limited surface-sensitive remineralization effects to largely Na-based depositions. Although cross-sectional mapping was not performed on specimens from this group, the SR X-ray CT data, including the corresponding HAP mineral concentrations, demonstrate an inductive effect lasting until about 900 nm. This effect was sustained at the lowest mineral concentration

among the three fluoride treatments, and may be limited kinetically due to due to of the relatively slower dissolution properties of the water-free varnish relative to the water-based prophy paste and dentifrice systems. As speculated above for the prophy paste and dentifrice, once a stop-gap process stabilized the tubule, permeation of ions and minerals deeper into the tubules was able to proceed. Among the three fluoride treatments, the relatively steep mineral concentration-depth slope lasting through depths ~ 3 μm may reflect the relatively higher NaF loading of the varnish system. Interestingly, a second plateau is observed around 3.5 μm, at which point the concentration increases appear similar to those provided by the dentifrice. In this region, the mineralization differences between the modalities appear immaterial, and suggests the properties of the tubules, including permeation and composition, may respond similarly. We note this 5% NaF varnish also includes a tailored functionalized TCP ingredient optimized for the varnish system [26,48], and the combination of these agents have been shown to deliver acid-resistant remineralization benefits [26,30-34,48]. Thus, it seems the remineralizing effect delivered by the varnish favored the tubular subsurface regions, at least as far as 4 μm, where elution of mineralizing ions from the sticky, slowly dissolving resin-based system appear to penetrate into demineralized regions. Similar to the dentifrice's effect on tubules, we note that despite tubular increases in mineral concentration, tubule occlusion was not necessarily observed. As discussed above for the dentifrice, the absence of tubule occlusion suggests another mechanism may be contributing to in vivo relief of dentinal hypersensitivity [2,4]. And, as commented on for the dentifrice, future studies can probe the cross-sectional elemental composition of the remineralized specimens. In view of the exploratory nature of this study, the SR X-ray CT results clearly reveal the remineralization effect of the varnish system and are consistent with laboratory and clinical findings of varnish efficacy [30-34].

Conclusion

The present study appears to be the first to probe the depth-dependence of tubular and intertubular regions of sound and demineralized dentin at submicron resolution. This was made possible due to the innovations in SR X-ray CT methodologies available at the Japan Synchrotron Radiation Research Institute. Additionally, this is the first SR X-ray CT study to resolve distinct regions of demineralized dentin treated with different fluoride modalities, including a prophy paste, dentifrice and varnish. Region-specific LAC values were then used to estimate mineral concentrations as a function of dentin depth. Additional microscopy techniques were also used to probe dentin structure and composition. Importantly, the use of SR X-ray CT to probe region-specific processes provides important insight into dentinal structure and may find further applications in addressing and understanding dentinal hypersensitivity.

Additional Information

1. Submicron CT, tubular dentin rendering example: https://youtu.be/8w-HjM616fI

Description: This corresponds to composition-contrast volume rendering for samples from groups S, D and C obtained by submicron CT. CTvox software (Bruker microCT, Belgium) was used to reconstruct 3D representations. Group C specimen representation was performed using the inversed contrast mode in order to visualize tubular dentin.

2. Sample A, EsB: https://youtu.be/Efxu8HhSFoQ

Description: This corresponds to composition-contrast volume renderings for the sample A specimen cross-section obtained via FIB. ATRAS 3D and Amira software were used to reconstruct 3D representations from EsB. A snapshot of this rendering is shown in Figure 17.

3. Sample A, SESI: https://youtu.be/q4Cnyv7bx_U

Description: This corresponds to composition-contrast volume renderings for the sample A specimen cross-section obtained via FIB. ATRAS 3D and Amira software were used to reconstruct 3D representations from SESI. A snapshot of this rendering is shown in Figure 17.

4. Sample D, EsB: https://youtu.be/asb01KkFH04

Description: This corresponds to composition-contrast volume renderings for the sample D specimen cross-section obtained via FIB. ATRAS 3D and Amira software were then used to reconstruct 3D representations from EsB.

5. Sample D, SESI: https://youtu.be/sw0PW4Qa66I

Description: This corresponds to composition-contrast volume renderings for the sample D specimen cross-section obtained via FIB. ATRAS 3D and Amira software were then used to reconstruct 3D representations from SESI.

Acknowledgments

We thank our patients provided extracted bicuspids for dentin specimen at Dr.Tetsuya Kuga dental practice, Dr. Masaya Nomura dental practice, Dr. Hisashi Yamakura dental practice and Dr. Makoto Asaizumi orthodontic practice. The authors kindly thank Dr. Yasuhito Kinjo at Tokyo Metropolitan Industrial Technology Research Institute (TIRI), whose provisional testing efforts helped serve as a basis for this ongoing research. We gratefully appreciate the advice from Dr. Naoto Yagi on sample preparation, CT experimental setup and FIB milling. Keyence VHX-500 was used in the Facilities Utilization program at TIRI. Dr. Kenichi Shimizu who is honorary professor at Keio University and visiting professor at Osaka city University advised sample preparation, FE-SEM selection and SE2 and In-lens detector selection. Mr. Masahiro Kaneseki helped perform statistical analyses. The synchrotron radiation experiments were performed at the BL47XU of SPring-8 with the approval of the Japan Synchrotron Radiation Research Institute (JASRI) (Proposal No. 2014B1049).

Conflicts of Interest

Dr. Karlinsey helped develop and has a business relationship regarding the commercial products studied in this manuscript. Miss. Oode, Drs. Asaizumi, Kato, Kuga, and Messrs. Oda, Sakurada, Tomson and Tabara declare no conflicts of interest.

Bibliography

1. Addy M and Smith S R. "Dentin Hypersensitivity: An overview on which to base tubule occlusion as a management concept". *Journal of Clinical Dentistry* 21.2 (2010): 25-30.

2. Gillam D G., *et al.* "The dentin disc surface: A plausible model for dentin physiology and dentin sensitivity evaluation". *Advances in Dental Research* 11.4 (1997): 487-501.

3. Pashley D H. "Dynamics of the pulpo-dentin complex". *Critical Reviews in Oral Biology and Medicine* 7.2 (1996): 104-133.

4. West N X., *et al.* "Dentin hypersensitivity: pain mechanisms and aetiology of exposed cervical dentin". Clinical Oral Investigations 17 (2013): S9-S19.

5. Goldberg M., *et al.* "Dentin: Structure, Composition and Mineralization". *Frontiers in Bioscience* 1.3 (2011): 711-735.

6. Pashley D H. "Dentin permeability, dentin sensitivity, and treatment through tubule occlusion". *Journal of Endodontics* 12.10 (1986): 465-474.

7. Pashley D H., *et al.* "Dentin hypersensitivity: Consensus-based recommendations for the diagnosis and management of dentin hypersensitivity". *Inside Dentistry* 4.9 (2008): 1-40.

8. Bevenius J., *et al.* "The micromorphology in vivo of the buccocervical region of premolar teeth in young adults: A replica study by scanning electron microscopy". *Acta Odontologica Scandinavica* 52.6 (1994): 323-334.

9. Rimondini L., *et al.* "Ultrastructure of hypersensitive and non-sensitive dentine". *Journal of Clinical Periodontology* 22.12 (1995): 899-902.

10. Rassameemasmaung S., *et al.* "The presence of fluid through dentin in periodontally-treated teeth". *Mahidol Dental Journal* 27.2 (2007): 99-106.

11. Flannery B P., *et al.* "Three-dimensional X-ray microtomography". *Science* 237.4821 (1987): 1439-1444.

12. Bonse U and Busch F. "X-ray computed microtomography (mictoCT) using synchrotron radiation (SR)". *Progress in Biophysics and Molecular Biology* 65(1-2) (1996): 133-169.

13. Willmott N S., *et al.* "An X-ray microtomography study on the mineral concentration of carious dentine removed during cavity preparation in deciduous molars". *Caries Research* 41.2 (2007): 129-134.

14. Ahmed M. "An X-ray microtomography study to validate the efficacies of caries removal in primary molars by hand excavation and chemo-mechanical technique". *Caries Research* 46.6 (2012): 561-567.

15. Clementino-Luedemann T N R., *et al.* "Micro-computed tomographic evaluation of a new enzyme solution for caries removal in deciduous teeth". *Dental Materials Journal* 25.4 (2006): 675-683.

16. Park YS., *et al.* "Theory of X-ray microcomputed tomography in dental research: application for the caries research". *Journal of the Korean Academy of Conservative Dentistry* 36.2 (2011): 98-107.

17. Zabler S., *et al.* "Fresnel-propagated submicrometer x-ray imaging of water-immersed tooth dentin". *Optics Letters* 32.20 (2007): 2987-2989.

18. Takeuchi A., *et al.* "Present status of the nanotomography system at BL47XU at Spring-8 and its efficiency improvement using double-condenser optics". *Journal of Physics Conference Series* 301.1 (2011): 1365.

19. Suzuki Y., *et al.* "Hard X-ray imaging microscopy using X-ray guide tube as beam condenser for field illumination". *Journal of Physics Conference Series* 463.1 (2013): 12028.

20. Tsuchiyama A., *et al.* "Analytical dual-energy microtomography: A new method for obtaining three-dimensional mineral phase images and its application to Hayabusa samples". *Geochimica et Cosmochimica Acta* 116 (2013): 5-16.

21. Asaizumi M., *et al.* "In vitro assessments of white-spot lesions treated with NaF plus tricalcium phosphate (TCP) toothpastes using synchrotron radiation micro computed tomography (SR micro CT)". *Journal of Dentistry and Oral Hygiene* 6.1 (2014): 10-21.

22. Uesugi K., *et al.* "Development of micro-tomography system with Fresnel zone plate optics at Spring-8". *Proceedings of SPIE* 6318 (2006): 63181F.

23. Takeuchi A., *et al.* "Zernike phase-contrast x-ray microscope with pseudo-Kohler illumination generated by sectored (polygon) condenser plate". *Journal of Physics Conference Series* 186.1 (2009): 12020.

24. Asaizumi M., *et al.* "In vitro assessments of white-spot lesions treated with NaF plus tricalcium phosphate (TCP) toothpastes using micro tomography (micro-CT)". *Journal of Dentistry and Oral Hygiene* 5.7 (2013): 68-76.

25. Karlinsey R.L., *et al.* "Remineralization potential of 5,000 ppm fluoride dentifrices evaluated in a pH cycling model". *Journal of Dentistry and Oral Hygiene* 2.1 (2010): 1-6.

26. Karlinsey RL and Pfarrer AM. "Fluoride plus functionalized β-TCP: A promising combination for robust remineralization". *Advances in Dental Research* 24.2 (2012): 48-52.

27. Amaechi BT., *et al*. "In situ remineralization of early caries by a new high-fluoride dentifrice". *General Dentistry* 60.4 (2012): e186-e192.

28. Mannaa A., *et al.* "Effects of high-fluoride dentifrice (5,000-ppm) on caries-related plaque and salivary variables". *Clinical Oral Investigations* 18.5 (2014): 1419-1426.

29. Mannaa A., *et al.* "Caries-risk profile variations after short-term use of 5000 ppm fluoride toothpaste". *Acta Odontologica Scandinavica* 72.3 (2014): 228-234.

30. Karlinsey RL., *et al.* "Noncontact remineralization of incipient lesions treated with a 5% sodium fluoride varnish in vitro". *Journal of Dentistry for Children* 81.1 (2014): 7-13.

31. Karlinsey RL., *et al.* "Effects on dentin treated with eluted multi-mineral varnish *in vitro*". *The Open Dentistry Journal* 6 (2012): 157-163.

32. Elkassas D and Arafa A. "Remineralizing efficacy of different calcium-phosphate and fluoride based delivery vehicles on artificial caries like enamel lesions". *Journal of Dentistry* 42.4 (2014): 466-474.

33. Pitchika V., *et al.* "Effectiveness of a new fluoride varnish for caries prevention in pre-school children". *Journal of Clinical Pediatric Dentistry* 38.1 (2013): 7-12.

34. Hammad S and Abdellatif A. "Effects of three different topical agents on enamel demineralization around orthodontic brackets: A clinical study". *Journal of Dental and Oral Health* 2.2 (2016): 33.

35. Asaizumi *et al.* "Observations of enamel microstructure in incipient lesions remineralized by NaF dentifrices". *Dental Research Management* 1.1 (2016): 19-29.

36. De Magalhães MF., *et al.* "Measurement of thermophysicalproperties of human dentin: Effect of open porosity". *Journal of Dentistry* 36.8 (2008): 588-594.

37. Burnett GW and Zenewitz JA. "Studies of the composition of teeth: VIII. The moisture content of calcified tooth tissues". *Journal of Dental Research* 37.4 (2010): 581-589.

38. Burnett GW and Zenewitz JA. "Studies of the composition of teeth: VIII. The composition of human teeth". *Journal of Dental Research* 37.4 (2010): 590-600.

39. Omokanwaye T and Wilson Jr O. "Ties that bind: Evaluation of collage I and α-chitin". *IFMBE Proceedings* 32 (1958): 183-187.

40. Berger MJ., *et al.* "XCOM: Photon Cross Section Database". National Institute of Standards and Technology.

41. Gysi A. "An attempt to explain the sensitiveness of dentine". *British Journal of Dental Science* 785.43 (1900): 865-868.

42. Misra DN. "Interaction of citric acid with hydroxyapatite: Surface exchange of ions and precipitation of calcium citrate". *Journal of Dental Research* 75.6 (1996): 1418-1425.

43. Lefèvre R., *et al.* "The study of human dentine with secondary ion microscopy and electron diffraction". *Calcified Tissue Research* 19 (1976): 251-261.

44. Marinho V C C., *et al.* "Topical fluoride (toothpastes, mouthrinses, gels or varnishes) for preventing dental caries in children and adolescents". *Cochrane Database of Systematic Reviews* 4 (2003): CD002782.

45. Karlinsey R L., *et al.* "*In vitro* assessments of experimental NaF dentifrices containing a prospective calcium phosphate technology". *American Journal of Dentistry* 22.3 (2009): 180-184.

46. Karlinsey R L., *et al.* "SEM evaluation of demineralized dentin treated with professional-strength NaF topical pastes". *American Journal of Dentistry* 24.6 (2011): 357-362.

47. Naoum S J., *et al.* "Enhancing fluoride mediated dentine sensitivity relief through functionalised tricalcium phosphate activity". *International Scholarly Research Notices* 2015 (2015): 905019.

48. Karlinsey R L., *et al.* "Preparation, characterization and *in vitro* efficacy of an acid-modified β-TCP material for dental hard-tissue remineralization". *Acta Biomaterialia* 6.3 (2010): 969-978.

Volume 5 Issue 2 September 2016